Chemical Physics Letters 734 (2019) 136726

Contents lists available at ScienceDirect

Chemical Physics Letters

journal homepage: www.elsevier.com/locate/cplett

Research paper

Substitution induced tunable emission of an airplane-like pyrene-based fluorophore: First-principles study

Tian Zhang[a,*], Sai Chu[a], Lili Lin[b], Chuan-Zeng Wang[a], Guangshuai Gong[a], Xiaojuan Song[a], Jianzhong Fan[b], Shuping Zhuo[a,*]

[a] School of Chemistry and Chemical Engineering, Shandong University of Technology, Zibo 255049, PR China
[b] Shandong Province Key Laboratory of Medical Physics and Image Processing Technology, School of Physics and Electronics, Shandong Normal University, Jinan 250014, PR China

HIGHLIGHTS

- Substitution effect on emission property of TBP2DPA has been theoretically studied.
- Emission becomes bluer and brighter with increasing electron negativity of group.
- Correlation between Hammett constant σ_p and emission property is well established.

ARTICLE INFO

Keywords:
Pyrene-based derivatives
Substitution effect
Excited-state properties
Tunable emission

ABSTRACT

The substitution effect on the optical emission properties of an airplane-like pyrene-based fluorophore is systematically investigated based on first-principles calculations. It is found that functional modification at the *para* position to the donor fragment allows for modulation of both the emission color and quantum efficiency. As the electron negativity of the substituent is increased, the luminescence becomes blue-shifted and brighter. The correlation between the Hammett substituent constant and emission properties has been well established, which provides a predictive strategy for the rational design of efficient and full-color pyrene-based fluorescent emitters.

1. Introduction

Pyrene is a typical polycyclic aromatic hydrocarbon (PAH) with four fused aromatic rings, which was initially used as the building block for the dye industry [1]. Nowadays, pyrene-based derivatives have attracted considerable interest for their tremendous utilities in the fields of organic electronics [2–5], chemosensing [6] and bioimaging [7,8]. Great efforts have been made to tune their emission behaviors for the development of new-generation organic optoelectronic devices [9]. The efficient pyrene-based materials with full-color emission are highly desired. The presence of donor-acceptor (D-A) moiety plays a crucial role in the fine-tuning of the optical properties based on intramolecular charge transfer (ICT) [10]. Recently, Yamato et al. have reported a D-A type pyrene-based fluorophore (TBP2DPA, Fig. 1), with the linkage between the donor of two diphenylamine (DPA) units and the acceptor of one *tert*-butylpyrene (TBP) core [11]. Facile substitution at the *para* position to its donor fragment allows for modification of the electronic structure and thus the photophysical properties. With decreasing the electron-donating ability of the substituents, tunable emission color from yellow to blue was achieved in dichloromethane solution. The relationship between the electron negativity of functional groups and the emission wavenumber has been established. Inspired by the experimental guidance, the unknown luminescence properties by appending electron-withdrawing substituents arouse our curiosity. Except for the emission color, the substitution effect on the emission quantum efficiency is still elusive. The primary purpose of this study is to elucidate the influence of adding substituents to the donor fragment on their respective optical emission properties.

In this work, we carried out theoretical studies on the excited-state properties of the substituted derivatives in solution (Fig. 1). Structural modification was made on the donor block with commonly used electron-donating substituents (NH_2, OCH_3, CH_3) and electron-withdrawing ones (F, CF_3 and CN), respectively. Both the emission maxima and excited-state decay rate constants were computed at the first-principles level. Our study gains deeper insights into the substitution induced tunable emission of such an interesting airplane-like pyrene-based

* Corresponding authors.
E-mail addresses: tzhang@sdut.edu.cn (T. Zhang), zhuosp_academic@yahoo.com (S. Zhuo).

https://doi.org/10.1016/j.cplett.2019.136726
Received 18 July 2019; Received in revised form 25 August 2019; Accepted 26 August 2019
Available online 27 August 2019

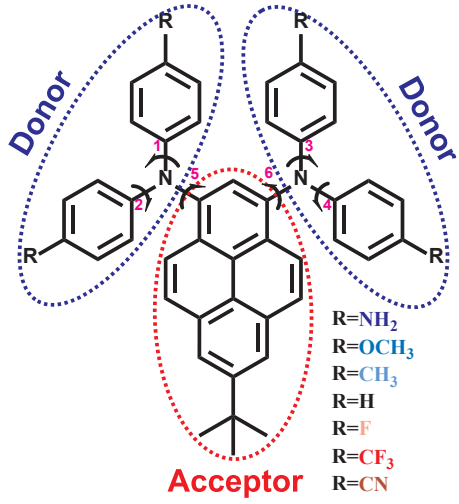

Fig. 1. Molecular structures of D-A type pyrene-based derivatives. The substituent naming with grading color shows its electron-donating/withdrawing ability (in blue/red). (For interpretation of the references to color in this figure legend, the reader is referred to the web version of this article.)

fluorophore.

2. Theoretical method

Density functional theory (DFT) and time-dependent DFT (TD-DFT) were used to perform electronic structure calculations in the ground (S_0) and first singlet excited state (S_1), respectively. The PBE0/6-31G(d) level [12] was adopted for geometry optimizations since it has been benchmarked to be reliable in dealing with singlet excited states of organic fluorophores [13]. It is known that TD-DFT calculations employing conventional functionals such as PBE0 usually underestimate the transition energies of CT states [14], due to the low percentage of Hartree-Fork exchange (HF%) in them. By contrast, the functionals with high HF% would induce excess excitation energy. As the investigated systems are typical D-A type molecules, we then tested different functionals and recomputed the vertical emission energies based on the optimized structures. Results for the case of OCH_3-substituent were presented in Table S1. It is found that the value obtained by the MPW1B95 [15] functional best matches the experimental emission maximum. Therefore, we adopted MPW1B95/6-31G(d) level to calculate the following transition properties of all investigated derivatives. The dichloromethane solvent was mimicked through the polarizable continuum model (PCM) with the help of Gaussian 16 package [16]. The equilibrium solvation approach was employed in both geometry optimizations and frequency calculations, and the non-equilibrium one was applied to compute vertical transition properties [17]. The emission quantum efficiency (Φ_f) is determined by both the radiative and non-radiative decay rate constants (k_r and k_{nr}). k_{nr} includes the internal conversion and intersystem crossing rate constants (k_{ic} and k_{isc}). Since the spin-orbit coupling (SOC) constants between the S_1 and T_1 states are quite small (0.12–0.34 cm^{-1}) for these derivatives (Table S2), as calculated in the BDF program [18], we ignore k_{isc} and only consider k_{ic} in the non-radiative decay process.

k_r can be computed through the Einstein spontaneous emission equation:

$$k_r = \frac{f\Delta E_{vert}^2}{1.499\ s\cdot cm^{-2}} \quad (1)$$

where f is the dimensionless oscillator strength, ΔE_{vert} is the vertical emission energy with the dimension of cm^{-1}.

The analytical formalism [19,20] we applied to obtain k_{ic} is written as:

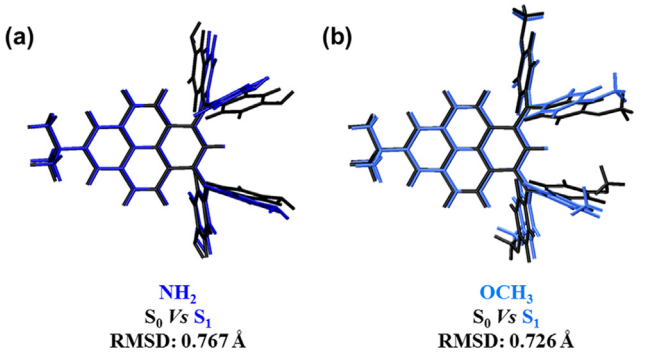

Fig. 2. Geometric comparisons between S_0 (in black) and S_1 (in blue) states for NH_2- (a) and OCH_3-substituted (b) derivatives in solution. (For interpretation of the references to color in this figure legend, the reader is referred to the web version of this article.)

$$k_{ic} = \sum_{kl} \frac{1}{\hbar^2} R_{kl} \int_{-\infty}^{\infty} [e^{i\omega_{if}t} Z_i^{-1} \rho_{ic,kl}(t, T)]\,dt \quad (2)$$

where $\rho_{ic,kl}(t, T)$ is the correlation function and Z_i is the partition function. R_{kl} represents the non-adiabatic electronic coupling matrix element that can be evaluated based on the first-order perturbation theory following Lin [21]. k_{ic} can be calculated in the MOMAP program [22]. The Lorentz broadening width (FWHM) of 10.62 cm^{-1} was adopted in all k_{ic} calculations following Niu [20], to ensure convergence of the correlation function.

3. Results and discussion

As shown in the previous study [23], geometric difference between the optimized S_0 and S_1 states plays an important role in the excited-state properties. Therefore, we plotted the intuitive geometric comparisons for these derivatives in Fig. 2 and Fig. S1. The root mean square displacement (RMSD) with the expression $RMSD = \sqrt{\frac{1}{N}\sum_i^{natom} [(x_i - x_i')^2 + (y_i - y_i')^2 + (z_i - z_i')^2]}$, was used to quantitatively characterize the geometric modification between two states, as can be calculated in the VMD program [24]. It is easily found that geometric changes are mainly located in the DPA donor part (1,2,3,4-positions in Fig. 1). The locations between donor and acceptor (5,6-positions) are also specifically noted because they can significantly affect the ICT property. Detailed geometric parameters related to above torsional motions are listed in Table S3. The RMSD values of NH_2- and OCH_3-substituents are 0.767 Å and 0.726 Å respectively, which are much greater than those of the others (0.096–0.340 Å). Torsional angles at 5,6-positions of the NH_2-substituent show biggest variations of ~14° and ~18° from S_0 to S_1 state, even more than those of the OCH_3-substituent (~9° and ~6°). Those at 1,2,3,4-positions of both NH_2- and OCH_3-substituents experience large changes with an average of ~10°. However, all dihedral angles exhibit minor modifications (most < 5°) in the other substituents, which implies less geometry relaxations in the non-radiative energy dissipation process.

Calculated transition properties for each substituted derivative are presented in Table 1, as well as the Hammett substituent constant σ_p [25]. σ_p has a positive correlation with the electron negativity of the functional group *para* on the phenyl. Electron-donating groups possess negative σ_p values. And likewise, positive σ_p values imply electron-withdrawing groups. The calculated vertical emission energies (ΔE_{vert}) reproduce well the available experimental band maxima, and the largest deviation is only 0.05 eV. As the σ_p value or the electron negativity of the substituent is increased, the predicted ΔE_{vert} rises swiftly at first and then goes up slowly (Fig. 3). A minor exchange was found for the H- and F-substituent, with quite close σ_p values. The lone pairs of the F-substituent may partially compensate its electron negativity. That exchange also exists in the following parameters. However, they are all

Table 1
Hammett constant for the substituent *para* on the phenyl σ_p, calculated adiabatic excitation energy ΔE_{ad} and vertical emission energy ΔE_{vert} for $S_1 \rightarrow S_0$, as well as the available experimental (exp.) emission peak value (in eV and nm), HOMO (H) → LUMO (L) component, overlap integral S of norm of HOMO and LUMO, electric transition dipole moment μ (in Debye) and oscillator strength f for the substituted derivatives in solution.

Substituent	σ_p	ΔE_{ad}	ΔE_{vert}	exp.[a]	H → L	S	μ	f
NH_2	−0.66	2.37 (523)	1.96 (633)	N. A.	98.4%	0.3392	3.55	0.09
OCH_3	−0.27	2.61 (475)	2.39 (519)	2.36 (525)	97.1%	0.6094	5.74	0.30
CH_3	−0.17	2.71 (458)	2.56 (484)	2.54 (489)	97.2%	0.7280	6.93	0.47
H	0.00	2.78 (446)	2.64 (470)	2.65 (467)	96.9%	0.7714	7.29	0.53
F	0.06	2.77 (448)	2.62 (473)	2.67 (465)	97.0%	0.7607	7.15	0.51
CF_3	0.54	2.90 (428)	2.74 (453)	N. A.	97.0%	0.8244	8.01	0.67
CN	0.66	2.92 (425)	2.74 (453)	N. A.	97.3%	0.8269	8.39	0.73

[a] Measured in dichloromethane, Ref. [11].

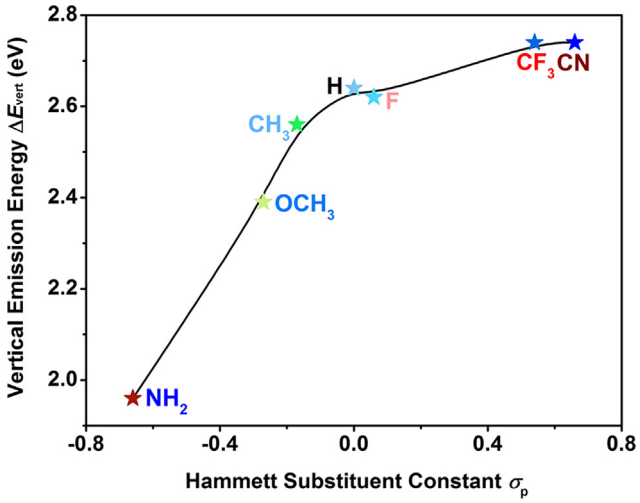

Fig. 3. Vertical emission energy ΔE_{vert} versus Hammett substituent constant σ_p for the substituted derivatives in solution. Colored star displays their respective emission color. (For interpretation of the references to color in this figure legend, the reader is referred to the web version of this article.)

trivial and hardly affect the main conclusion. Based on the analysis of excitation components, the S_1 states are dominated by the HOMO → LUMO transitions. The contours of HOMOs and LUMOs, as well as their energy gaps are shown in Fig. 4. The NH_2-substituent exhibits obvious ICT from the *para*-substituted DPA donor to the TBP acceptor. The ICT induces severe orbital separation and the reddest emission. The HOMO-LUMO energy gap is remarkably enlarged and then gradually reaches a plateau with increasing the electron negativity of the substituent, in accord with ΔE_{vert}. The electron-donating group (NH_2, OCH_3, CH_3) attached to the donor fragment can strengthen the D nature of the D-A architecture and promote ICT, resulting in the fast modification of energy gap and ΔE_{vert}. On the contrary, the electron-withdrawing group (F, CF_3 and CN) attenuates the ICT in part, leading to somewhat local excitation (LE) feature. The overlap between HOMO and LUMO can be quantified by their norm integral S, as can be calculated in the Multiwfn program [26]. It can be seen that the S value of the NH_2-substituent is smallest (~0.34) and tends to be greater with the increased σ_p value. The electric transition dipole moment μ and oscillator strength f keep pace with S because $\mu = \iint \phi_L(1)\phi_H(2)\ r_{12}\ \phi_L(2)\phi_H(1)d\tau_1 d\tau_2$ and $f \sim \mu^2$.

Calculated room-temperature k_r and k_{ic} values were listed in Table 2. The k_r value of the substituted derivative is progressively elevated with the rising σ_p value due to the enhanced f and blue-shifted ΔE_{vert} according to Eq. (1), whereas the k_{ic} value falls suddenly then gradually decreases. An exception is the alternate sequence of the H- and F-substituent, as also stated previously. Either increasing k_r or decreasing k_{ic} could give rise to high emission efficiency because $\Phi_F \approx k_r/(k_r + k_{ic})$. As a result, Φ_f ascends in the order of $NH_2 \ll OCH_3 < CH_3 < F < H < CF_3 < CN$, as determined from both calculated and available experimental results. The correlation between σ_p and Φ_f is shown in Fig. 5, quite similar to the relationship between σ_p and ΔE_{vert}. Bluer and brighter emission can be obtained with increasing the electron negativity of the substituent. Although the calculated Φ_f values are slightly underestimated compared to the existing experimental measurements, the tunable and predictable optical emission properties are expected. To fully address this issue, an explicit solvent model deserves future investigation [27].

To gain deeper insight into the non-radiative decay process, we plotted the log (k_{ic}) parabola versus the energy gap ΔE in Fig. S2. The k_{ic} value corresponds to the vertical coordinate when ΔE locates at the

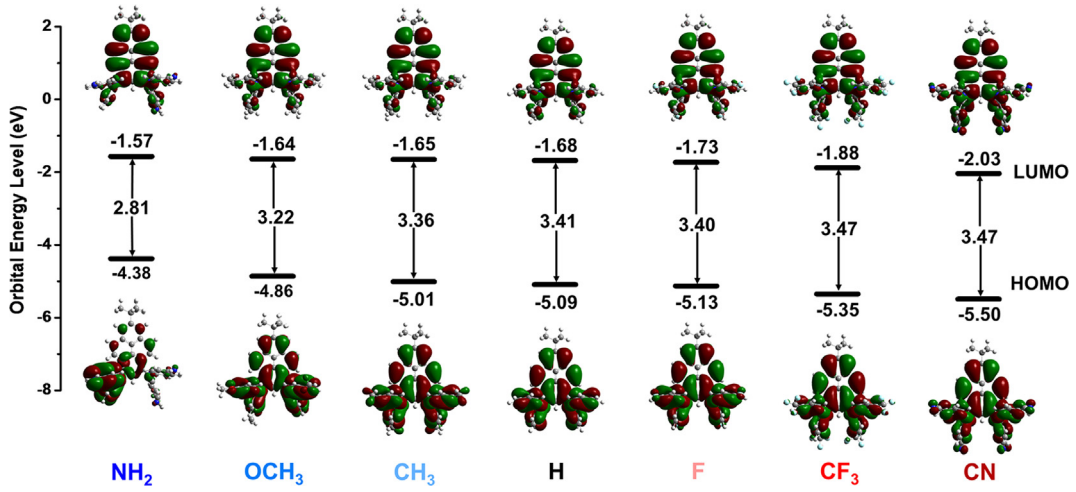

Fig. 4. Energy levels and electron density distributions of HOMOs and LUMOs for the substituted derivatives at their S_1-optimized geometries in solution.

Table 2
Calculated k_r (s^{-1}), k_{ic} (s^{-1}) and Φ_f values for the substituted derivatives in solution. Available experimental Φ_f values are given in parentheses.

Substituent	σ_p	k_r	k_{ic}	Φ_f
NH_2	−0.66	1.5×10^7	1.0×10^{11}	0.015% (N.A.)
OCH_3	−0.27	7.4×10^7	7.8×10^7	48.7% (60.0%)
CH_3	−0.17	1.3×10^8	4.9×10^7	72.6% (78.0%)
H	0.00	1.6×10^8	4.1×10^7	79.6% (82.0%)
F	0.06	1.5×10^8	4.4×10^7	77.3% (79.0%)
CF_3	0.54	2.2×10^8	3.5×10^7	86.3% (N.A.)
CN	0.66	2.4×10^8	2.8×10^7	89.6% (N.A.)

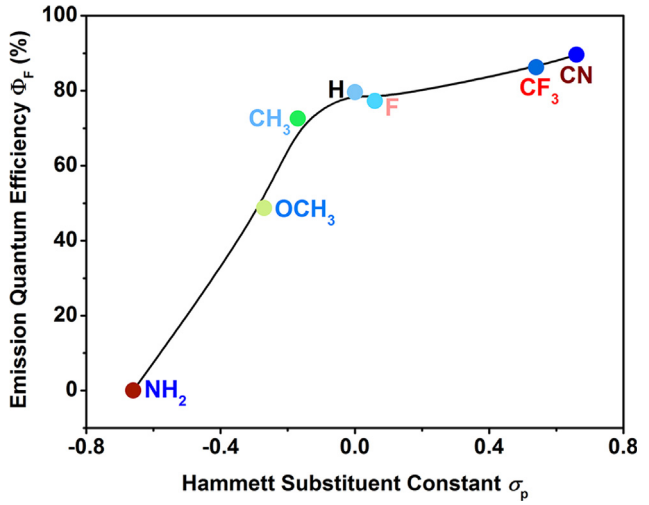

Fig. 5. Emission quantum efficiency Φ_f versus Hammett substituent constant σ_p for the substituted derivatives in solution.

adiabatic excitation energy ΔE_{ad} (Table 1). According to the k_{ic} formula in Eq. (2), the pre-factor R_{kl} can accelerate k_{ic} and the breadth of the log (k_{ic}) parabola increases with the total relaxation energy λ [21,28]. Energy gap law tells us small ΔE_{ad} favors large k_{ic} as log (k_{ic}) decreases nearly linearly with ΔE, when ΔE is large enough. The diagonal parts R_{kk} of R_{kl} for each substituted derivative are shown in Fig. S3. It is found that R_{kk} hardly varies upon substitution, leading to almost unaffected k_{ic} via electronic coupling. We can see from Fig. S2 that the log (k_{ic}) parabola of the NH_2-substituent is much broader than the others with similar breadth. The total λ values for all substituted derivatives are listed in Table S4. The largest λ of the NH_2-substituent can greatly broaden the parabola and enlarge its k_{ic} value to 11 orders of magnitude, leading to the non-luminescent emission. For the others with relatively small λ, the energy gap law governs. It can be seen ΔE_{ad} increases in the order of OCH_3 < CH_3 < F < H < CF_3 < CN, which is consistent with the decreasing sequence of the k_{ic} values.

λ quantifies the vibrations' ability to accept the excited-state electronic energy [29]. Under the harmonic oscillator approximation, λ_j of each normal mode can be defined as $\lambda_j = \hbar S_j \omega_j = \frac{1}{2} D_j^2 \omega_j^2$. S_j is the Huang-Rhys factor for the j-th mode and D_j is the mode displacement between two electronic states. The sum of all modes is the total λ. The above normal mode analyses can be realized in the EVC module of the MOMAP program. λ_j versus the mode frequency ω_j are shown in Fig. 6 and Fig. S4, taking NH_2-, OCH_3-, H- and CF_3-substituents for examples. It can be seen that the two vibration regions, *i.e.*, low-frequency (LF, < 200 cm^{-1}) and high-frequency (HF, 1400–1800 cm^{-1}), are major contributions in the vibrational relaxation process. The relaxation energies of LF and HF modes for all derivatives are presented in Table S4. The LF contribution is quite outstanding (234 meV) for the NH_2-substituent, minor (86 meV) for the OCH_3-substituent and tiny (14–41 meV) for the others. These LF modes are mainly assigned to the out-of-plane twisting motions. However, the HF contribution exhibits minor change with modification of the substituent, and the HF modes belong to the mixed vibrations of CC stretching and CH in-plane bending.

4. Conclusions

In conclusion, we have conducted a theoretical study on the optical emission properties of a D-A type pyrene-based derivative in solution. The effect of *para*-substitution in the donor fragment on the excited-state properties is systematically investigated. It is found that the emission becomes blue-shifted and brighter with increasing the electron negativity of the substituent. The calculated emission wavelength and quantum efficiency of OCH_3-, CH_3-, H- and F-substituents agree well with the available experiments. The NH_2-substituent is predicted to be non-emissive. The CF_3- and CN-substituents are theoretically designed to be blue emitters with high efficiency. The correlation between the Hammett substituent constant and emission properties provides a predictive strategy for modulation of the photophysical properties in the D-A type pyrene-based fluorophores. Through analysis of the non-radiative relaxation energy projected onto vibrational modes, the torsional motions involved in the low-frequency modes are significant dissipation channels for the NH_2-substituent, resulting in the largest k_{ic} value with 11 orders of magnitude. For the other substituents, the energy gap law governs the luminescence order. Our study provides instructive information for the molecular design of efficient organic fluorescent molecules with full-color emission.

Finally, we note that although the adopted methodology has shown successful in predicting the excited-state properties for a series of organic luminophores, including the pyrene-based derivatives in this work, quantitative prediction of the optical emission properties in

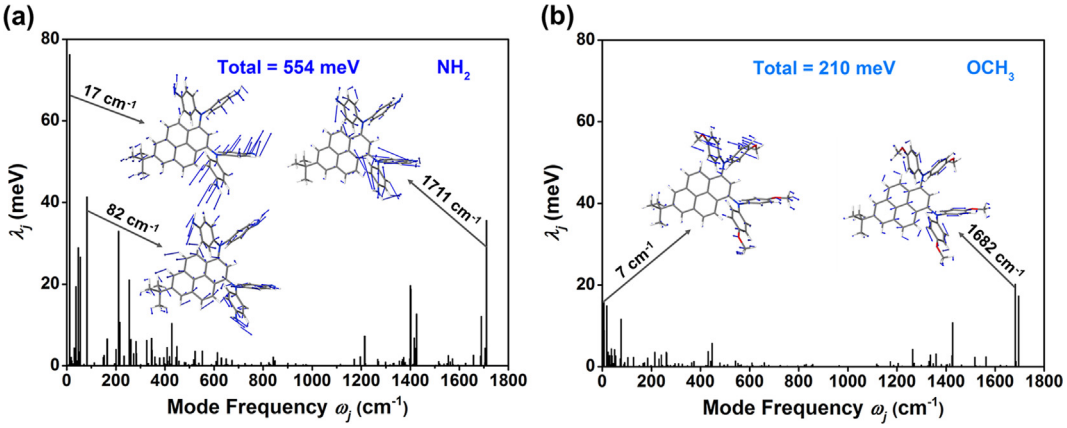

Fig. 6. Relaxation energy λ_j versus mode frequency ω_j for NH_2- (a) and OCH_3-substituted (b) derivatives in solution.

organic light-emitting materials is still challenging [30,31].

Declaration of Competing Interest

The authors declare that they have no known competing financial interests or personal relationships that could have appeared to influence the work reported in this paper.

Acknowledgement

This work is supported by the National Natural Science Foundation of China (Grant Nos. 21703122, 21576159, 11974216, 11904210) and the Natural Science Foundation of Shandong Province (Grant Nos. ZR2017BB034, ZR2019MA056, ZR2019BB067).

Appendix A. Supplementary material

Supplementary data to this article can be found online at https://doi.org/10.1016/j.cplett.2019.136726.

References

[1] R.D. Welham, The early history of the synthetic dye industry. I. The chemical history, J. Soc. Dyers Color 79 (1963) 98–105.
[2] T.M. Figueira-Duarte, K. Müllen, Pyrene-based materials for organic electronics, Chem. Rev. 111 (2011) 7260–7314.
[3] D. Chercka, S.J. Yoo, M. Baumgarten, J.J. Kim, K. Müllen, Pyrene based materials for exceptionally deep blue OLEDs, J. Mater. Chem. C 2 (2014) 9083–9086.
[4] Y.B. Gong, X.J. Zhan, Q.Q. Li, Z. Li, Progress of pyrene-based organic semiconductor in organic field effect transistors, Sci. China Chem. 59 (2016) 1623–1631.
[5] M.M. Islam, Z. Hu, Q. Wang, C. Redshaw, X. Feng, Pyrene-based aggregation-induced emission luminogens and their applications, Mater. Chem. Front. 3 (2019) 762–781.
[6] G. Lin, H. Ding, D. Yuan, B. Wang, C. Wang, A pyrene-based, fluorescent three-dimensional covalent organic framework, J. Am. Chem. Soc. 138 (2016) 3302–3305.
[7] M.E. Shirbhate, Y. Jeong, G. Ko, G. Baek, G. Kim, Y.-U. Kwon, K.M. Kim, J. Yoon, Selective fluorescent recognition of Zn^{2+} by using chiral binaphthol-pyrene probes, Dyes Pigm. 167 (2019) 29–35.
[8] V. Srinivasan, M.A. Jhonsi, N. Dhenadhayalan, K.-C. Lin, D.A. Ananth, T. Sivasudha, R. Narayanaswamy, A. Kathiravan, Pyrene-based prospective biomaterial: *In vitro* bioimaging, protein binding studies and detection of bilirubin and Fe^{3+}, Spectrochim. Acta A 221 (2019) 117150.
[9] J. Yang, Q. Guo, X. Wen, X. Gao, Q. Peng, Q. Li, D. Ma, Z. Li, Pyrene-based blue AIEgens: tunable intramolecular conjugation, good hole mobility and reversible mechanochromism, J. Mater. Chem. C 4 (2016) 8506–8513.
[10] J. Gu, X. Li, Z. Zhou, R. Liao, J. Gao, Y. Tang, Q. Wang, Synergistic regulation of effective detection for hypochlorite based on a dual-mode probe by employing aggregation induced emission (AIE) and intramolecular charge transfer (ICT) effects, Chem. Eng. J. 368 (2019) 157–164.
[11] C.Z. Wang, H. Ichiyanagi, K. Sakaguchi, X. Feng, M.R.J. Elsegood, C. Redshaw, T. Yamato, Pyrene-based approach to tune emission color from blue to yellow, J. Org. Chem. 82 (2017) 7176–7182.
[12] C. Adamo, V. Barone, Toward reliable density functional methods without adjustable parameters: the PBE0 model, J. Chem. Phys. 110 (1999) 6158–6170.
[13] D. Jacquemin, V. Wathelet, E.A. Perpète, C. Adamo, Extensive TD-DFT benchmark: singlet-excited states of organic molecules, J. Chem. Theory Comput. 5 (2009) 2420–2435.
[14] A. Dreuw, M. Head-Gordon, Single-reference ab initio methods for the calculation of excited states of large molecules, Chem. Rev. 105 (2005) 4009–4037.
[15] Y. Zhao, D.G. Truhlar, Hybrid meta density functional theory methods for thermochemistry, thermochemical kinetics, and noncovalent interactions: the MPW1B95 and MPWB1K models and comparative assessments for hydrogen bonding and van der waals interactions, J. Phys. Chem. A 108 (2004) 6908–6918.
[16] M.J. Frisch, G.W. Trucks, H.B. Schlegel, G.E. Scuseria, M.A. Robb, J.R. Cheeseman, G. Scalmani, V. Barone, G.A. Petersson, H. Nakatsuji, X. Li, M. Caricato, A.V. Marenich, J. Bloino, B.G. Janesko, R. Gomperts, B. Mennucci, H.P. Hratchian, J.V. Ortiz, A.F. Izmaylov, J.L. Sonnenberg, D. Williams-Young, F. Ding, F. Lipparini, F. Egidi, J. Goings, B. Peng, A. Petrone, T. Henderson, D. Ranasinghe, V.G. Zakrzewski, J. Gao, N. Rega, G. Zheng, W. Liang, M. Hada, M. Ehara, K. Toyota, R. Fukuda, J. Hasegawa, M. Ishida, T. Nakajima, Y. Honda, O. Kitao, H. Nakai, T. Vreven, K. Throssell, J.A. Montgomery Jr., J.E. Peralta, F. Ogliaro, M.J. Bearpark, J.J. Heyd, E.N. Brothers, K.N. Kudin, V.N. Staroverov, T.A. Keith, R. Kobayashi, J. Normand, K. Raghavachari, A.P. Rendell, J.C. Burant, S.S. Iyengar, J. Tomasi, M. Cossi, J.M. Millam, M. Klene, C. Adamo, R. Cammi, J.W. Ochterski, R.L. Martin, K. Morokuma, O. Farkas, J.B. Foresman, D.J. Fox, Gaussian16 Revision B.01, Gaussian, Inc., Wallingford, CT, 2016.
[17] J. Tomasi, B. Mennucci, R. Cammi, Quantum mechanical continuum solvation models, Chem. Rev. 105 (2005) 2999–3094.
[18] Z.D. Li, Y.L. Xiao, W.J. Liu, On the spin separation of algebraic two-component relativistic hamiltonians, J. Chem. Phys. 137 (2012) 154114.
[19] Q. Peng, Y.P. Yi, Z.G. Shuai, J.S. Shao, Toward quantitative prediction of molecular fluorescence quantum efficiency: role of Duschinsky rotation, J. Am. Chem. Soc. 129 (2007) 9333–9339.
[20] Y.L. Niu, Q. Peng, C.M. Deng, X. Gao, Z.G. Shuai, Theory of excited state decays and optical spectra: application to polyatomic molecules, J. Phys. Chem. A 114 (2010) 7817–7831.
[21] S.H. Lin, Rate of interconversion of electronic and vibrational energy, J. Chem. Phys. 44 (1966) 3759–3767.
[22] Y.L. Niu, W.Q. Li, Q. Peng, H. Geng, Y.P. Yi, L.J. Wang, G.J. Nan, D. Wang, Z.G. Shuai, MOlecular MAterials Property Prediction Package (MOMAP) 1.0: a software package for predicting the luminescent properties and mobility of organic functional materials, Mol. Phys. 116 (2018) 1078–1090.
[23] J. Fan, L. Lin, C.-K. Wang, Excited state properties of non-doped thermally activated delayed fluorescence emitters with aggregation-induced emission: a QM/MM study, J. Mater. Chem. C 5 (2017) 8390–8399.
[24] W. Humphrey, A. Dalke, K. Schulten, VMD: Visual molecular dynamics, J. Mol. Graph. Model. 14 (1996) 33–38.
[25] C. Hansch, A. Leo, R.W. Taft, A survey of Hammett substituent constants and resonance and field parameters, Chem. Rev. 91 (1991) 165–195.
[26] T. Lu, F. Chen, Multiwfn: a multifunctional wavefunction analyzer, J. Comput. Chem. 33 (2012) 580–592.
[27] N. De Mitri, S. Monti, G. Prampolini, V. Barone, Absorption and emission spectra of a flexible dye in solution: a computational time-dependent approach, J. Chem. Theory Comput. 9 (2013) 4507–4516.
[28] S.H. Lin, C.H. Chang, K.K. Liang, R. Chang, Y.J. Shiu, J.M. Zhang, T.S. Yang, M. Hayashi, F.C. Hsu, Ultrafast dynamics and spectroscopy of bacterial photosynthetic reaction centers, Adv. Chem. Phys. 121 (2002) 1–88.
[29] T. Zhang, W. Shi, D. Wang, S. Zhuo, Q. Peng, Z.G. Shuai, Pressure-induced emission enhancement in hexaphenylsilole: a computational study, J. Mater. Chem. C 7 (2019) 1388–1398.
[30] W.Q. Li, L.L. Zhu, Q. Shi, J.J. Ren, Q. Peng, Z.G. Shuai, Excitonic coupling effect on the nonradiative decay rate in molecular aggregates: formalism and application, Chem. Phys. Lett. 683 (2017) 507–514.
[31] Z.G. Shuai, Q. Peng, Organic light-emitting diodes: Theoretical understanding of highly efficient materials and development of computational methodology, Natl. Sci. Rev. 4 (2017) 224–239.